FINITE ELEMENT SIMULATION OF THE STRUCTURAL RESPONSE OF ADOBE MASONRY BUILDINGS SUBJECTED TO LATERAL LOADING

Rogiros Illampas, Dimos C. Charmpis, and Ioannis Ioannou

Department of Civil and Environmental Engineering, University of Cyprus,
P.O. Box 20537, 1678 Nicosia, Cyprus
e-mail: {rilamp01, charmpis, ioannis}@ucy.ac.cy

Keywords: Adobe masonry, FE modelling, non-linear analysis, damaged plasticity, structural response, horizontal loading

Abstract. *This paper examines the use of Finite Element (FE) continuum macro-models for the assessment of the structural behaviour of unreinforced adobe masonry structures subjected to horizontal thrusts. For the purpose of validating FE numerical models, a 1:2 scaled replica of an existing single-storey traditional adobe building was constructed and subjected to monotonic static lateral loading. The modes of failure sustained under the imposition of significantly high horizontal forces were noted during the tests, while cracking initiation and propagation were macroscopically recorded. Based on the experimental results, damage limit states at different levels of deformation were identified. In the framework of numerical investigation, a detailed 3D FE model was developed. This was used for performing non-linear analyses, aiming to simulate the general response of the structure under test. For the numerical representation of adobe masonry, a damaged plasticity constitutive law was adopted, while experimentally derived material data were used as input parameters (i.e. modulus of elasticity, material behaviour under compression and tension, etc.). The validity of the numerical results was verified both qualitatively and quantitatively through comparisons with the experimental damage patterns and force-displacement curves. The numerical investigation conducted enabled the identification of the factors, which critically affect the FE simulation of earthen structures.*

1 INTRODUCTION

The large stock of historic adobe structures surviving to-date constitutes a significant feature of the international architectural heritage. At the same time, buildings composed of unfired earth are still erected in many developing countries, while efforts are being made to introduce adobes to contemporary sustainable architecture as alternative low-cost, environmentally-friendly materials.

Several experimental studies examining the structural behaviour of adobe construction have been conducted (e.g. [1-5]). Both dynamic and static laboratory tests have been implemented on full- or reduced-scale wall configurations and model buildings. Research on the computational analysis of adobe structures has generally been less systematic and has focused on the development of continuum FE models [6-8] and discrete element models [8-10] through the use of existing constitutive laws.

The current study combines laboratory testing with non-linear numerical analysis to examine the use of FE models for the simulation of laterally loaded unreinforced adobe masonry structures. For the purpose of FE model calibration, a scaled adobe structure was subjected to static horizontal loading tests. The experimental data obtained provided useful information regarding the prevalent failure mechanisms and enabled the identification of damage limit states at different levels of deformation. Adopting a macro-modelling approach and a continuum damaged plasticity material model, the behaviour of the tested structure was successfully simulated using FE analysis. The use of appropriate modelling parameters is hereby discussed, while the factors which critically affect the analysis of adobe masonry construction are noted.

2 EXPERIMENTAL INVESTIGATION OF THE STRUCTURAL RESPONSE OF A SCALED ADOBE BUILDING

2.1 Test set-up and instrumentation

The model structure examined at the Structures Laboratory of the University of Cyprus (Fig. 1a) is a 1:2 scaled replica of a Cypriot single-storey vernacular dwelling. For its construction, scaled-down adobe bricks sized (height x width x length) 30 x 150 x 220 mm^3 were laid in a running bond pattern using earth mortar (composition soil:straw:water $\approx$ 200:6:100 w/w). The joints' thickness was kept below 10 mm in accordance with the local traditional building technique. The model's walls were 220 mm thick.

Figure 1: (a) The 1:2 scaled adobe building tested at the Structures Laboratory of the University of Cyprus. (b) The hydraulic jack and the timber beam used for imposing lateral loads on the structure's rear wall.

The model structure was built indoors upon a fixed timber base. Its external dimensions were (width x length) 1.75 x 3.60 m^2. The height of the front elevation was 1.50 m, while that of the rear wall was 1.65 m. A door 1.10 m high and 0.70 m wide was formed on the façade. Windows measuring 0.55 x 0.55 m^2 were created at the two side walls. On the rear wall, a triangular ventilation notch 0.22 m wide and 0.18 m high was formed.

The first layer of bricks was set on the base with the application of mortar. Horizontal translations at this level were constrained by timber elements installed at the perimeter of the walls. Connection between intersecting walls was achieved by means of overlapping bricks.

Timber lintels composed of two jointed 85 x 85 mm^2 beams were installed above all openings. Nine timber rafters, 45 x 90 mm^2 in cross-section, were placed at regular intervals to span the space between the two opposite longitudinal walls. To account for the weight of roof tiles, adobes were uniformly placed on a 20 mm-thick wooden panel that was nailed upon the rafters. The abutments of the lintels and rafters were set into the masonry with gypsum mortar.

Testing commenced nine weeks after the completion of the construction and involved the application of monotonically increasing lateral forces. Loading was exerted along the length of the rear wall at approximately 2/3 of the structure's height. The load-imposition system consisted of a timber beam and a 60 kN-capacity hydraulic jack with a swivel head (Fig. 1b).

Linear Variable Differential Transducers (LVDTs) (range ± 50.8 mm, accuracy ± 0.25%) were used for recording the displacements generated at one of the side walls and at the two adjacent halves of the longitudinal walls. During the tests it was verified that there was close analogy between the response of the sections monitored and of the parts symmetric to them. Displacement measurements conducted at the base confirmed that no translation or rotation at this level took place. Damage evolution was monitored using digital cameras.

2.2 Experimental results

The recorded mode of damage is shown in Fig. 2. Cracks were observed at the rear and the two side walls. No visible damage was detected at the façade or at any of the timber members. Damage localization is attributed to the concentration of stresses at certain load-bearing elements due to inability of the structure to develop integral box action.
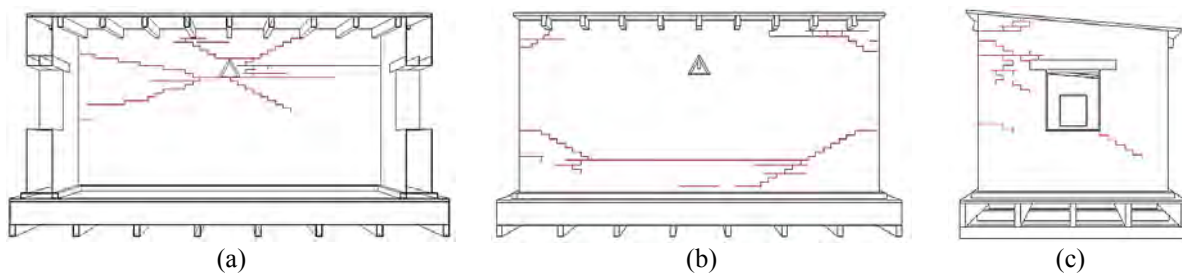

| (a) | (b) | (c) |

Figure 2: Cracking patterns recorded at the interior (a) and exterior (b) surfaces of the rear wall and at the side wall (c) after the imposition of lateral loads on the model building.

A major horizontal crack, parallel to the line of loading (Fig. 2a), was formed at the interior of the rear wall due to out-of-plane bulging. Overstressing at the load imposition point caused the development of diagonal cracks that extended from the centre of the rear wall towards its two lower sides.

Out-of-plane bending led to the development of a continuous horizontal crack along the exterior base of the rear wall (Fig. 2b). Damage towards the two sides followed an inclined path due to the partial restrain imposed by the orthogonal walls. The considerable deformation of the rear wall caused the concentration of high stresses at areas where masonry was in con-

tact with much stiffer timber rafters. As a result, cracks at the vicinity of the roofs' supports were generated. In addition, failure of the gypsum mortar joints at the rafters' abutments and subsequent sliding of the roof was noted.

The two side walls that sustained in-plane loads developed diagonal shear cracks that radiated out of the openings' corners and extended throughout the whole width of the masonry (Fig. 2c). Damage propagated through the joints and spread towards the rear wall, eventually joining with the cracks formed below the roof rafters. At the final stages of the experimental procedure, the side walls' upper sections were subjected to out-of-plane torsional movement.

Crack formation was characterized by failure at the brick-mortar interface due to weak adhesion among the masonry constituents. This is in line with the comments of [1, 2, 11-13]. The recorded crack opening was significant ranging from 5 to 20 mm. Forms of damage similar to those hereby described have also been reported in other studies [2, 4, 14-19]. However, seismic failure modes involving separation of intersecting walls could not be reproduced through the unilateral and monotonic load imposition process applied. Moreover, a distribution of out-of-plane loads to all sections perpendicular to the direction of the principal action that would be representative of a dynamic state could not be achieved because static loads could not be effectively transferred from the rear wall to the façade through the insufficiently bonded rafters. Instead, movement of the façade was dictated by the in-plane drift of the two side walls and no noticeable damage (i.e. cracking and/or detachment) developed.
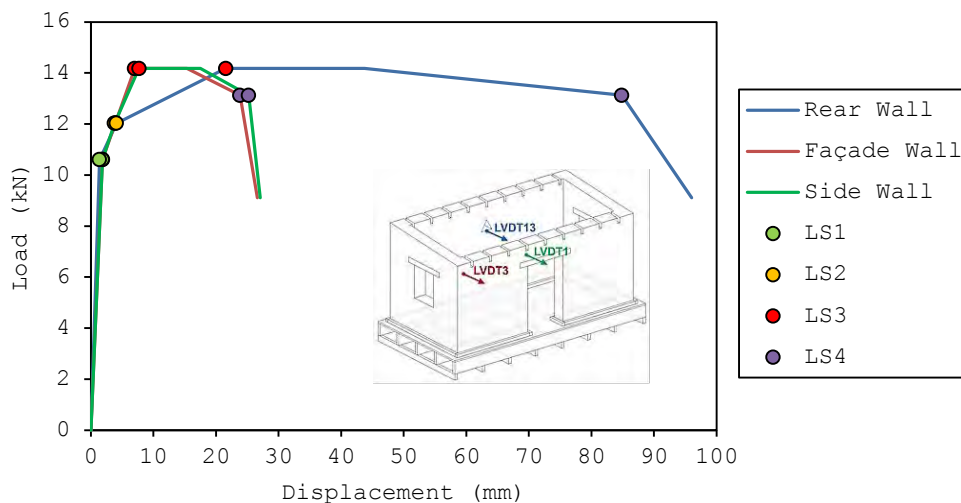

Figure 3: Force-displacement data obtained from monitoring transversal movement at the upper sections of the façade, side and rear walls. Four damage limit states (LS1-4) are denoted at different levels of deformation.

Fig. 3 presents the variation of the displacements measured at the upper sections of the rear, side and façade walls in relation to the load imposed. Associating the recorded force-displacement response with the corresponding state of damage, four limit states (LS1-4) have been identified. Consistent response to horizontal loading with no or negligible damage of the masonry was maintained up to 5% of the total displacement capacity and 75% (10.6 kN) of the maximum lateral resistance (LS1). At this stage, the displacements recorded at monitoring points were 1.8 mm and account for a lateral drift (= horizontal displacement / monitoring point's vertical distance from building's base) of 0.11%.

At loads exceeding 10.6 kN, cracking developed at the interior of the rear wall and at the two side walls and a reduction of the overall stiffness was noted. However, the structure was able to function as a homogeneous structural system up to 11% of its total displacement ca-

pacity and 85% (12 kN) of its maximum lateral resistance (LS2). At LS2, a coinstantaneous movement of 4 mm of all monitoring points and a lateral drift of 0.26% were recorded.

Up to LS3, where the structure attained its maximum lateral resistance (14.2 kN), further cracking, permanent distortion, considerable reduction of the overall stiffness, loss of interaction between the load-bearing members and differential movement of the masonry walls were noted. At this stage, pre-existing fissures extended in length, new cracks were formed at the base of the rear wall and sliding failure at the roof rafters' supports occurred. The displacements measured at the façade and side walls were 7 and 7.7 mm, respectively. In terms of lateral drift, these values can be interpreted as 0.5%. The out-of-plane translation at the centre of the rear wall was 21.6 mm, which accounts for a lateral drift of 1.4%.

From LS3 to LS4, structural behaviour was characterized by depletion of the overall stiffness and by inability to sustain higher levels of loading. Crack opening attained its maximum value (≈ 20 mm) and relatively small augments of the imposed load could generate large in- and out-of-plane drifts. At LS4 the horizontal translation of the side wall was 23.8 mm and that of the façade was 25.2 mm. The lateral drift at these sections was 1.6%. The displacement of the rear wall was 84.9 mm, while the lateral drift at its central section was 5.7%.

Beyond LS4, an abrupt drop in the structure's lateral resistance was recorded. Extensive cracking led to the formation of a kinematic mechanism involving the rocking motion of the façade and of the two adjacent triangular halves of the side walls. The forces imposed on the rear section of the structure could be partially transferred to the frontal detached part through common contact points. Hence, the effective resisting area of the masonry was reduced and its overall bearing capacity fell to a residual value. The experimental procedure was terminated at this point without forcing the structure to total or partial collapse.

The damage limit states described above are in agreement with the data presented in [4] and [20]. The maximum load sustained by the tested structure accounts for approximately 30% of its total self-weight. This value is rather conservative compared to the 34-100% base shear force-to-weight ratios reported elsewhere [1, 3, 5, 21]. Considering, however, that the adopted test set-up precluded the development of certain failure mechanisms, it is anticipated that the capacity of the model building to resist reversing seismic loads is actually even lower.

3 CALIBRATION OF CONTINUUM FE MODEL

3.1 Modelling and analysis of the tested structure

The response of the tested scaled building was simulated in Abaqus/CAE. The walls, the lintels, the roof and the loading-beam were modelled as individual bodies interacting with each other. Since the test configuration is symmetric, the model developed represented only half the structure. All bodies were discretized using 8-noded 3D linear brick elements (C3D8). The model consisted of 4888 elements, 4998 nodes and involved 14994 degrees of freedom (Fig. 4).
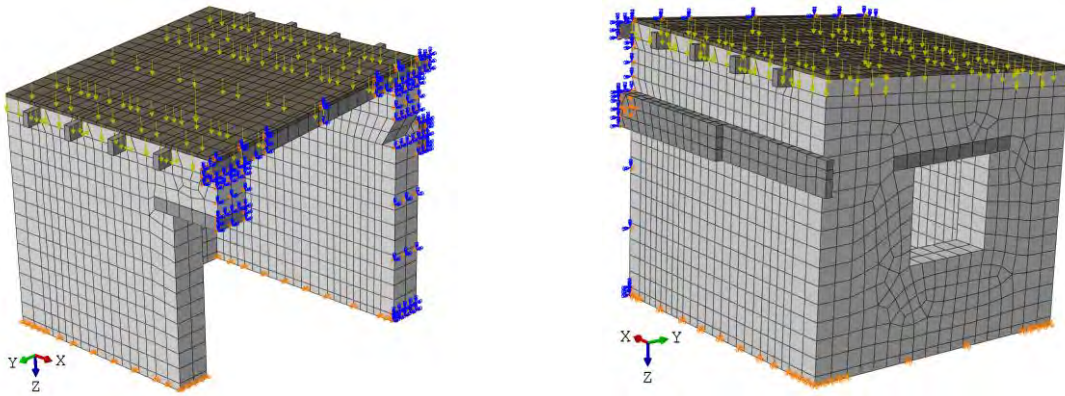
Figure 4: FE model developed for the simulation of lateral load tests on an adobe scaled building.

Numerical representation of adobe masonry followed a continuum macro-modelling approach. Masonry was idealized as a fictitious homogeneous medium and its behaviour was simulated with the concrete damaged plasticity constitutive model implemented in Abaqus/CAE [22]. The adopted model uses concepts of brittle fracture and isotropic damaged elasticity. It assumes that the inelastic response of a material is governed by tensile cracking and compressive crushing. Cracking and crushing are expressed by means of softening/hardening variables, which control the evolution of the yield surface.

Most parameters required for the constitutive modelling of adobe masonry were derived from experimental material data. Density was measured as $\rho = 1300$ kg/m^3. Poisson's ratio was evaluated as the ratio between the transversal and axial deformations recorded during the compressive strength testing of a stack-bonded masonry prism [23]; $v = 0.3$.

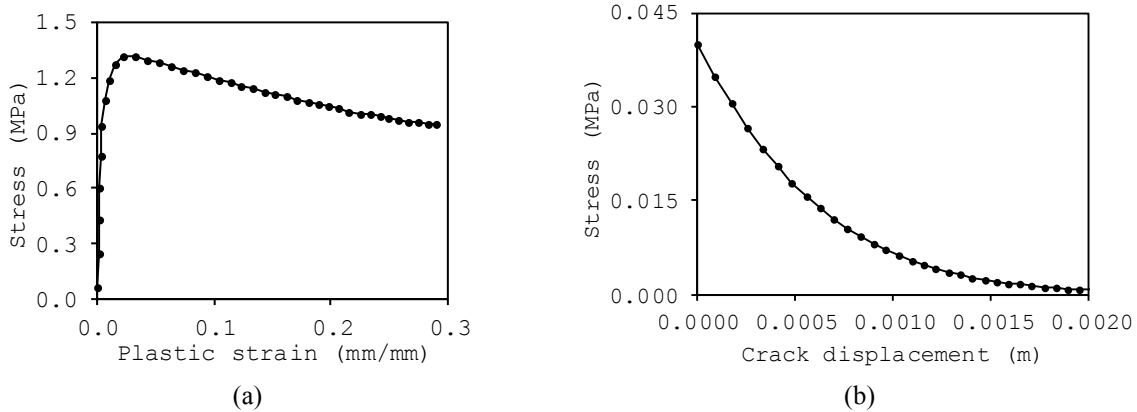(a)   (b)

Figure 5: Compressive stress-plastic strain and tensile stress-crack displacement input data specified for the homogenized adobe masonry in compression (a) and tension (b), respectively.

To define the response of masonry to compression, the relation developed in [24] for adobe bricks was adopted and compressive stresses were expressed as a function of plastic (crushing) strains (Fig. 5a). Compressive strength and strain at peak compressive stress were assessed from tests on stack-bonded prisms; $f_w = 1.3$ MPa, $\varepsilon_{cu} = 0.1$ mm/mm [25]. Considering that earth-based materials, such as adobes, possess a granular structure and have thus limited elastic response, non-linear behaviour was assumed at stresses exceeding 5% of the bearing capacity. Young's modulus was computed from the compressive stress-strain relation as a secant modulus up to the yielding point; $E = 18$ MPa.

6

In tension, softening behaviour was assigned by specifying stress-cracking displacement tabular data (Fig. 5b). Tensile stresses were computed as a function of the tensile strength f_t, the fracture energy G_f, the cracking strain ε_t^{ck} and the elements' characteristic crack length h according to the following relation [26]:

$$\sigma_t = f_t \exp\left(-\frac{hf_t}{G_f}\varepsilon_t^{ck}\right) \tag{1}$$

Tensile plastic strains were converted to equivalent cracking displacements using the elements' characteristic crack length.

Uniaxial tensile strength was defined as $f_t = 0.04$ MPa following the diagonal tension testing of an adobe wallette [23]. Tensile fracture energy was evaluated from the results reported in [27], where a 4.5 N/m average energy was required for inducing failure to adobe couplets with a mean tensile strength of 0.01 MPa. Assuming a linear analogy between the tensile strength and the fracture energy, $G_f = 18$ N/m was estimated for $f_t = 0.04$ MPa. The characteristic crack length $h = 100$ mm was computed as the cubic root of the product between the elements' dimensions (h_z, h_x, h_y) [28, 29]. The global size of the masonry elements' sides was set as 100 ± 10 mm to satisfy the energy criterion:

$$h \leq \frac{G_f E}{f_t^2} \tag{2}$$

The yield surface was fully defined by four additional plasticity characteristics. The rate at which the hyperbolic flow potential approaches its asymptote ($e = 0.1$) and the ratio between the initial equibiaxial and the initial uniaxial compressive yield stresses ($\sigma_{b0}/\sigma_{c0} = 1.16$) were adopted from [22]. Parameter K_c that affects the shape of the yield surface in the deviatoric plane was set equal to 0.8 according to the recommendations of [22] for soils modelled with a Drucker-Prager yield function. Based on [6] and [30], a minimal value of $\psi = 1^{\circ}$ was selected for the dilation angle controlling the plastic volumetric strain developed upon plastic shearing.

The timber members of the tested structure were modelled to exhibit linearly elastic and isotropic behaviour. The material parameters used were drawn from the literature [31, 32] and are as follows: (a) roof panel - density $\rho = 380$ kg/m^3; Young's modulus $E = 8000$ MPa; Poisson's ratio $v = 0.2$ and (b) openings' lintels, roof rafters and loading-beam - density $\rho = 670$ kg/m^3; Young's modulus $E = 7000$ MPa; Poisson's ratio $v = 0.3$.

Interaction among the masonry and the timber members in the normal direction was modelled using "hard" contact pressure-overclosure relationships that allowed for the transfer of any stress under compression but enforced separation under tension. In the tangential direction, a finite-sliding formulation that uses the Coulomb theory to compute shear stress as a function of the contact pressure and the interface's friction coefficient was adopted. The friction coefficient specified at the interfaces between the masonry and the openings' lintels and the masonry and the roof rafters was $\mu = 0.5$ [13]. The loading-beam and the roof panel were assumed to slide freely ($\mu = 0$) on the surface of the masonry.

All three translational degrees of freedom were constrained at the walls' base. Kinematic constrains were also imposed at the basal perimeter, where lateral movement was restrained by timber elements. Along the plane of symmetry, movement in the x direction and rotations around the y and z axes were not allowed. Constraints precluding translation along the x and z axes were defined at the nodes where the hydraulic jack was in contact with the timber loading-beam. At the same nodes, progressively increasing lateral displacements were imposed to simulate horizontal loading. The weight of the adobes placed upon the roof was evenly distributed over the panel's elements as an additional weight per unit volume.

The analysis was completed in two successive steps using a general non-linear static procedure with automatic stabilization. After applying the dead loads at the initial step, lateral loads were incrementally enforced at time intervals ranging from 1×10^{-19} to 1×10^{-4} s over a 1 s period. The effect of geometric non-linearities was accounted for in both numerical steps.

3.2   Comparisons between experimental-numerical results

The results of the analysis indicate that a good approximation of the structure's deformed shape was achieved (Fig. 6). In line with the experimental observations made, bulging develops at the area where loading is applied and thus the maximum lateral displacement occurs at the centre of the rear wall. The FE model also predicted an interrelation between the out-of-plane movement of the façade and the in-plane drift of the side wall. The displacements computed at these walls are approximately equal and show the same linear increase towards the top.
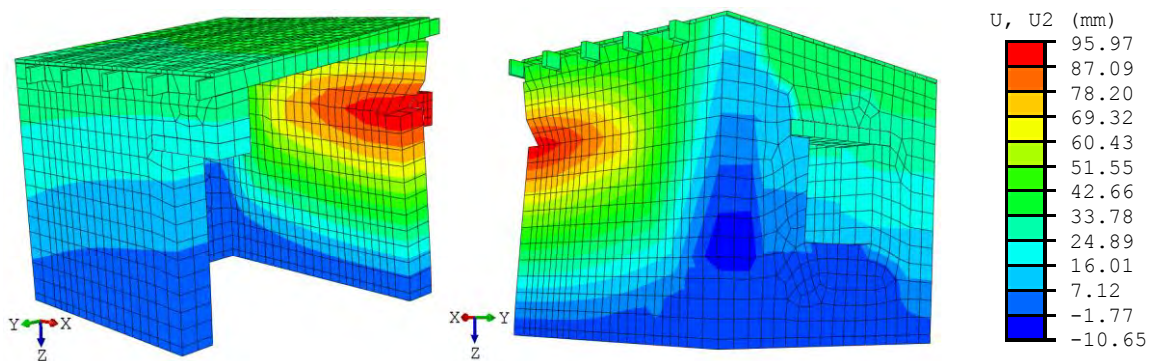

Figure 6: Contour representations of the computed distribution of lateral displacements.
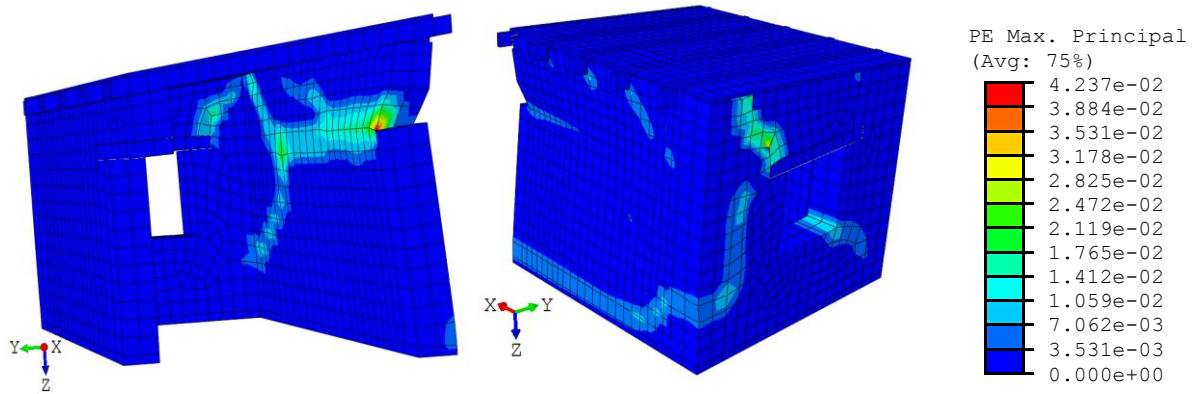

Figure 7: Contour diagrams with the maximum principal plastic strains computed.

The effective cracks predicted by the FE model are shown in Fig. 7. Crack prediction lies on the hypothesis that the direction of the vector normal to the crack plane is parallel to the direction of the maximum principal plastic strains [22]. Both the cracking pattern and the initiation-evolution of damage were adequately captured. At the initial stages of the simulation, rapid propagation of tensile plastic strains across a horizontal band at the rear wall's interior occurred. Soon afterwards, significantly high plastic strains that followed inclined paths were generated at the two opposite corners of the side wall's window opening. At higher levels of deformation, damage at the rear wall's interior extended diagonally from the principal line of failure towards the wall's upper and lower sections. Moreover, horizontal cracks developed at

the exterior base of the rear wall and at the vicinity of the roof's supports. The numerical model, however, overestimated the side wall's out-of-plane torsional movement and predicted the development of a near-vertical crack at its upper rear section.

A comparison between the experimental and numerical force-displacement curves is presented in Fig. 8 for the upper sections of the side, the façade and the rear walls. The numerical load data reported were estimated as the sum of all lateral contact forces generated at the nodes of the timber loading-beam. The experimental and numerical diagrams generally show the same trends. In both cases, a post-yield plateau, succeeded by a gradual reduction of the load-bearing capacity, is observed. However, the abrupt drop in load resistance that occurs in the experimental curves could not be captured. This is because physical separation between cracked sections of the masonry walls cannot be simulated by a homogenized continuum.

Reasonable agreement is found between the experimentally measured and the numerically computed maximum lateral resistance of the tested structure, as the two values differ only by 4.5%. The ultimate out-of-plane translation of the rear and façade walls' control nodal points was also successfully predicted. In this case, the difference between the experimental and numerical values is practically negligible, since it is below 2%. However, the FE analysis predicted a 29.6 mm lateral movement at the top of the side wall, instead of the test's 27.1 mm, thus overestimating this section's in-plane drift by 9.2%.
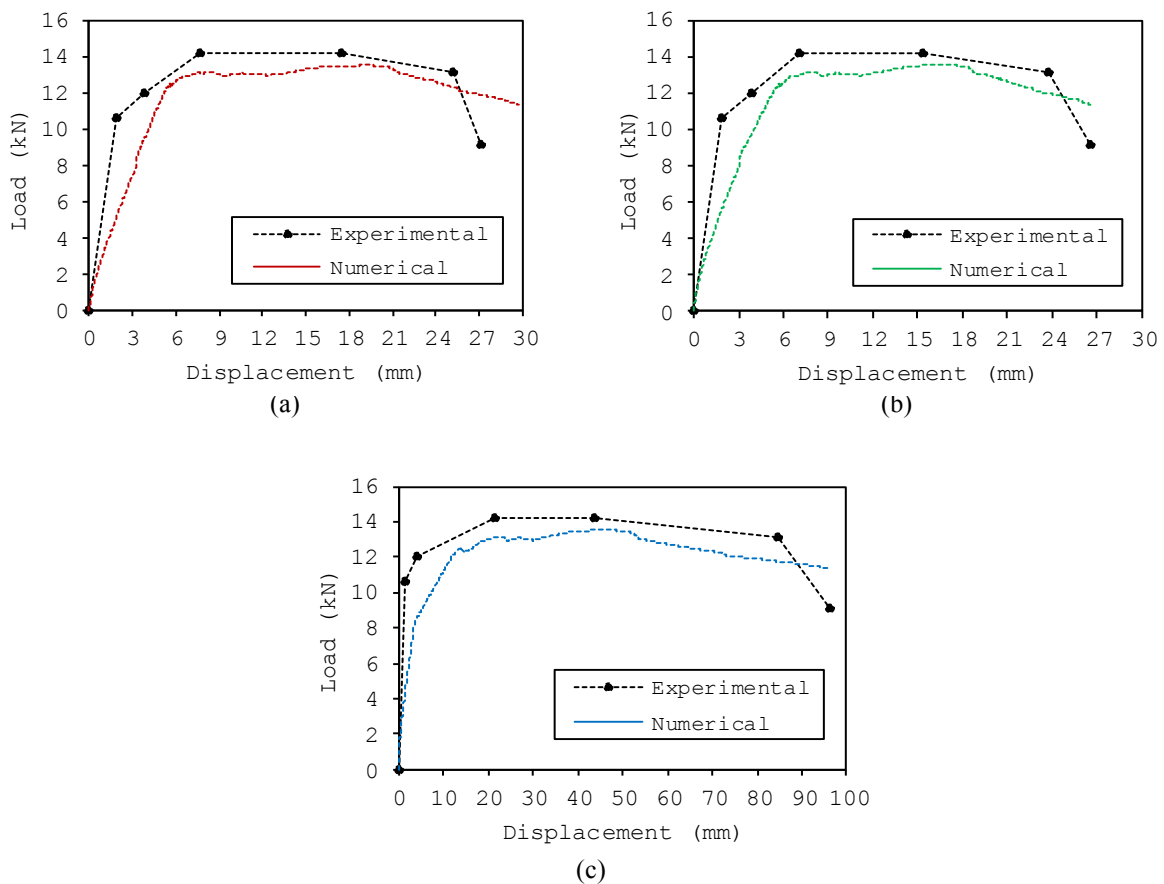

(a)

(b)

(c)

Figure 8: Comparison between experimental force-displacement data envelopes and corresponding numerical results for the upper sections of (a) the side, (b) the façade and (c) the rear walls.

Bearing in mind the inhomogeneity and randomness of earthen materials, the numerical results obtained are considered satisfactory. Good correlation among the computed distribution of plastic strains and the experimentally recorded damage pattern verifies the adequacy of the

FE model to simulate adobe masonry structural response. Of particular importance is also the ability of the FE model to predict the forces and displacements with sufficient accuracy. Some deviations that occur are primarily attributed to the generic limitations of continuum modelling and to the crude hypothesis of isotropic masonry damage imposed by the formulation of the adopted constitutive law.

A number of simulations conducted in the process of model calibration using different material properties, revealed that the predicted lateral resistance and deformation capacity are highly sensitive to variation of the stiffness (i.e. Young's modulus) and tension softening (i.e. tensile strength, fracture energy) parameters assigned to the masonry medium. The frictional properties assigned at the timber-masonry interfaces also affect, albeit to a smaller degree, the predicted global response, since they control the transfer of forces between the two materials, thus determining whether sliding of the roof rafters will occur. On the other hand, the compressive strength, the Poisson's ratio and the plasticity characteristics of the yield surface (e, σ_{b0}/σ_{c0}, K_c, ψ) were found to pose limited influence on the outcomes of the analysis.

Analogous conclusions concerning the effect of the various modelling parameters on the simulation of unreinforced adobe masonry construction can be found in [8]. This further highlights the importance of having experimentally derived material data, adequate for simulating all significant features of adobe masonry's structural behaviour.

4 CONCLUSION

The laboratory testing of a 1:2 scaled building showed that the response of unreinforced adobe construction to horizontal loading is characterized by tensile cracking failure due to weak bonding among the masonry units. The accumulated force-displacement data showed that homogeneous structural response is lost as soon as stiffness degradation occurs and differential movement of the walls takes place. This verifies that the absence of a stiff diaphragm configuration at roof level and the insufficient interaction between the various load-bearing members pose a negative effect on the structural behaviour of masonry buildings.

The damaged plasticity constitutive model hereby adopted was proven to be adequate for the computational analysis of adobe masonry structures. Provided that appropriate material data have been used and that proper calibration has been undertaken, continuum FE models can macroscopically capture the global behaviour of adobe buildings, approximating with adequate accuracy their force-displacement response and failure mode.

REFERENCES

[1] J. Ottazzi, J. Yep, M. Blondet, G. Villa-Garcia, J.F. Ginocchio, Shaking table tests of improved adobe masonry houses. *9th World Conference on Earthquake Engineering*, Tokyo-Kyoto, Japan, August 2-9, 1988.

[2] E.L. Tolles, H. Krawinkler, *Seismic studies on small-scale models of adobe houses*. John A. Blume Earthquake Engineering Center, Technical Report No. 91: Department of Civil and Environmental Engineering Stanford University, Stanford, 1990.

[3] B. Samali, W. Jinwuth, K. Heathcote, C. Wang, Seismic capacity comparison between square and circular plan adobe construction. *Procedia Engineering*, **14** (1), 2103-2108, 2011.

[4] A. Figueiredo, H. Varum, A. Costa, D. Silveira, C. Oliveira, Seismic retrofitting solution of an adobe masonry wall. *Materials and Structures*, **46** (1-2), 203-219, 2013.

[5] A.S. Bartolomé, E. Delgado, D. Quiun, Seismic behaviour of two storey model of confined adobe masonry. *11ᵗʰ Canadian Masonry Symposium*, Toronto, Ontario, Canada, 31 May - 3 June, 2009.

[6] N. Tarque, G. Camata, E. Spacone, H. Varum, M. Blondet, Elastic and inelastic parameters for representing the seismic in-plane behaviour of adobe wall. *11ᵗʰ International Conference on the Study and Conservation of Earthen Architectural Heritage Terra 2012*, Lima, Peru, April 22-27, 2012.

[7] N. Tarque, G. Camata, E. Spacone, H. Varum, M. Blondet, Non-linear dynamic analysis of a full-scale unreinforced adobe model. *Earthquake Spectra*, In-Press, doi: http://dx.doi.org/10.1193/022512EQS053M.

[8] N. Tarque, G. Camata, E. Spacone, H. Varum, M. Blondet, Numerical modelling of the in-plane behaviour of adobe walls. *8ᵗʰ National Conference on Seismology and Earthquake Engineering*, Aveiro, Portugal, October 20-23, 2010.

[9] A. Furukawa, Y. Ohta, Failure process of masonry buildings during earthquake and associated casualty risk evaluation. *Natural Hazards*, **49** (1), 25-51, 2009.

[10] Z. Cao, H. Watanabe, Earthquake response prediction and retrofitting techniques of adobe structures. *13ᵗʰ World Conference on Earthquake Engineering*, Vancouver, B.C., Canada, August 1-6, 2004.

[11] P. Walker, Bond characteristics of earth block masonry. *Journal of Materials in Civil Engineering*, **11** (3), 249-256, 1999.

[12] G. Azeredo, J.C. Morel, Tensile strength of earth mortars and its influence on earth masonry behaviour. *11ᵗʰ International Conference on Non-conventional Materials and Technologies (NOCMAT2009)*, Bath, UK, September 6-9, 2009.

[13] J. Kiyono, A. Kalantari, Collapse mechanism of adobe and masonry structures during the 2003 Iran Bam Earthquake. *Bulletin of the Earthquake Research Institute, University of Tokyo*, **79** (3/4), 157-161, 2004.

[14] E.L. Tolles, F.A. Webster, A. Crosby, E.E. Kimbro, *Survey of damage to historic adobe buildings after the January 1994 Northridge earthquake*. The Getty Conservation Institute, Los Angeles, 1996.

[15] E.L. Tolles, E.E. Kimbro, A.F. Webster, S.W. Ginnel, *Seismic stabilization of historic adobe structures: Final report of the Getty seismic adobe project*. Getty Conservation Institute, Los Angeles, 2000.

[16] Y. Yucheng, Y. Liu, Earthquake damage to and aseismic measures for earth-sheltered buildings in China. *Tunnelling and Underground Space Technology*, **2** (2), 209-216, 1987.

[17] R. Illampas, I. Ioannou, D.C. Charmpis, Overview of the pathology, repair and strengthening of adobe structures. *International Journal of Architectural Heritage*, **7** (2), 165-188, 2013.

[18] D. Torrealva, C. Cerrón, Y. Espinoza, Shear and out of plane bending strength of adobe walls externally reinforced with polypropylane grids. *14th World Conference on Earthquake Engineering*, Beijing, China, October 12-17, 2008.

[19] M. Blondet, J. Vargas, N. Tarque, Observed behaviour of earthen structures during the Pisco earthquake (Peru). *14th World Conference on Earthquake Engineering*, Beijing, China, October 12-17, 2008.

[20] N. Tarque, H. Crowley, R. Pinho, H. Varum, Seismic capacity of adobe dwellings. *14th European Conference on Earthquake Engineering*, Ohrid, FYROM, 30 August - 3 September, 2010.

[21] M. Blondet, I. Madueño, D. Torrealva, G. Villa-García, F. Ginocchio, Using industrial materials for the construction of safe adobe houses in seismic areas. *Earth Build 2005 Conference*, Sydney, Australia, January 19-21, 2005.

[22] SIMULIA CORP. *Abaqus 6.10 theory manual*. Dassault Systèmes, Rising Sun Mills, 2009.

[23] R. Illampas, *Experimental and computational investigation of the structural response of adobe structures*, PhD Thesis: Department of Civil and Environmental Engineering, University of Cyprus, 2013.

[24] R. Illampas, I. Ioannou, D.C. Charmpis, Adobe bricks under compression: Experimental investigation and derivation of stress–strain equation. *Construction and Building Materials*, **53** (28), 83-90, 2014.

[25] R. Illampas, I. Ioannou, D.C. Charmpis, A study of the mechanical behaviour of adobe masonry. *12th International Conference on Structural Repairs and Maintenance of Heritage Architecture*, Chianciano Terme, Italy, September 5-7, 2011.

[26] P.B. Lourenço, Anisotropic softening model for masonry plates and shells. *Journal of Structural Engineering*, **126** (9), 1008-1016, 2000.

[27] J.A.P.P. Almeida, *Mechanical characterization of traditional adobe masonry elements*. MSc Thesis: Department of Civil Engineering, University of Minho, 2012.

[28] A. Saetta, R. Scotta, R. Vitaliani, Coupled environmental-mechanical damage model of RC structures. *Journal of Engineering Mechanics*, **125** (8), 930-940, 1999.

[29] G. Creazza, R. Matteazzi, A. Saetta, R. Vitaliani, Analyses of masonry vaults: A macro approach based on three-dimensional damage model. *Journal of Structural Engineering*, **128** (5), 646-654, 2002.

[30] G.T. Houlsby, *How the dilatancy of soils affects their behaviour*. University of Oxford, Report Number OUEL 1888/91, Soil Mechanics Report 121/91, Department of Engineering Science, 1991.

[31] D.W. Green, J.E. Winandy, D.E. Kretschman, Mechanical properties of wood. R.J. Ross ed. *Wood handbook: Wood as an engineering material*. U.S. Department of Agriculture, Forest Service, Forest Products Laboratory, General Technical Report FPL-GTR-113, Madison WI, 1999.

[32] E.S. Katsaragakis, *Timber construction* [In Greek]. NTUA Publications, Athens, 2000.